Analysis of corrosion damage by Proctor et al.
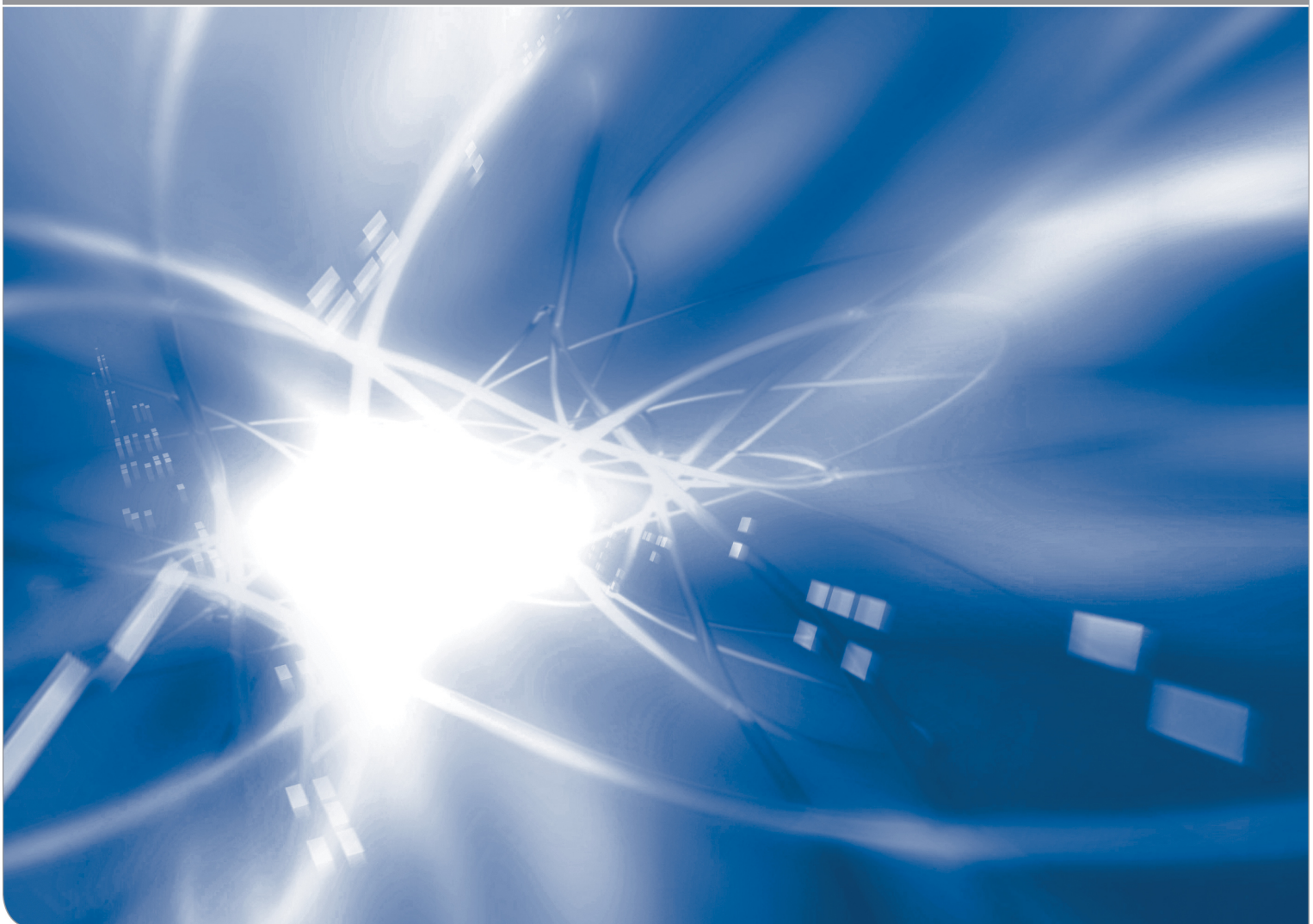
K.G. Schell, T. Fett, C. Bucharsky, G. Rizzi

IAM Institute for Applied Materials

Abstract

In a study by Proctor et al. a strength reduction was observed due to surface damaging in humid air at high temperatures. The strength tests on these damaged specimens were carried out in normal lab atmosphere. Unfortunately, these tests are affected by subcritical crack growth.

In the present report we show on the strength results obtained in humid air, in which way these data can be used to determine the inert strength of the damaged surface.

Proctor et al. provided images of the surface defects and identified, localized corrosion centers. In our report we show how the effects of these local corrosion defects can be handled fracture mechanically.

Contents

1. Surface damage by corrosion

1.1 Effect of treatment temperature

When silica surfaces undergo high temperature treatment in lab air, they are strongly damaged as can be concluded from strength measurements on silica fibres by Proctor et al. [1] and Lezzi et al. [2]. The strength data measured in normal lab air by Proctor [1] are shown for 30-40 min treated fibres as red circles in Fig. 1a. Figure 1b represents the same data with logarithmic ordinate scaling. The strengths by Lezzi for only 1 min heat treated fibres are represented as the squares with the standard deviation as the bars. Surface inspections after the strength tests by Proctor et al. [1] revealed the local damages from which final fracture started. According to the weakest link model, we have to expect that failure occurred at the most serious or largest damage. An example of such a surface damage for a heat-treatment time of 30-40 min at 800°C in lab air is shown in Fig. 2. From this image and a cross section image in [1] we can conclude that the corrosion event appears roughly as a hemisphere that is strongly cracked by irregularly oriented cracks. The thickness of the lines corresponds with the visibility of the crack patterns within the half-sphere. The right part of Fig. 2 includes the grey-distribution.
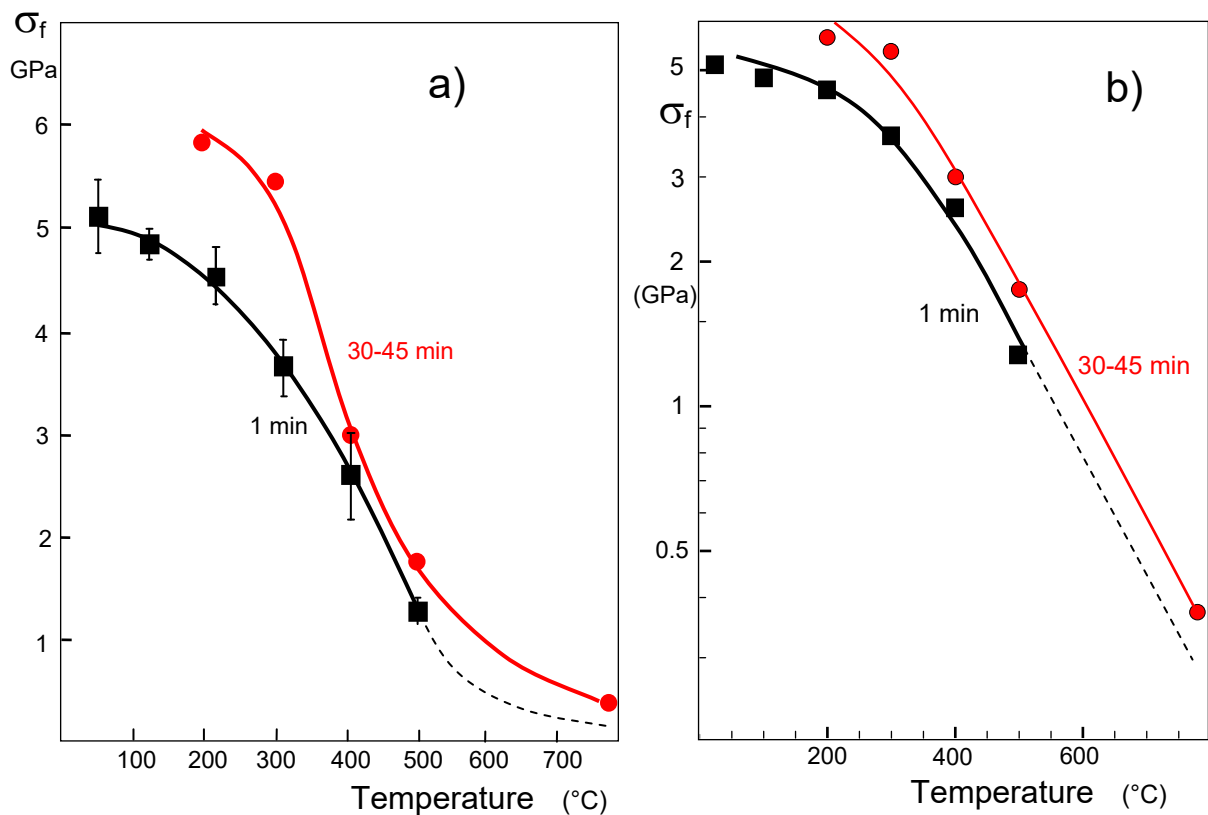

Fig. 1 Strength measurements by Proctor et al. [1] (red circles) and Lezzi et al. [2] (squares), a) linear ordinate, b) logarithmic ordinate scaling.
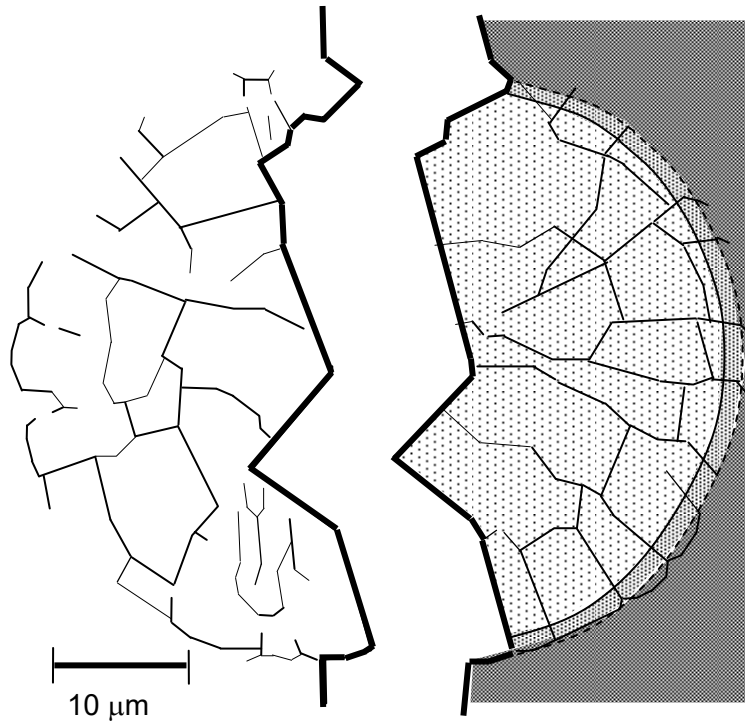
Fig. 2 Crack patterns within a nearly spherical surface damage according to Proctor et al. [1], left part: Cracks exclusively, right part: Shadowing included.

1.2 Effect of treatment time

The time-dependent strengths σ_f at 500°C from Proctor [1] are shown in Fig. 3. With increasing time, a monotonously decreasing strength was found.

Fig. 3 Strength of silica fibres in humid lab air as a function of treatment time at 500°C, measured by Proctor et al. [1].

2

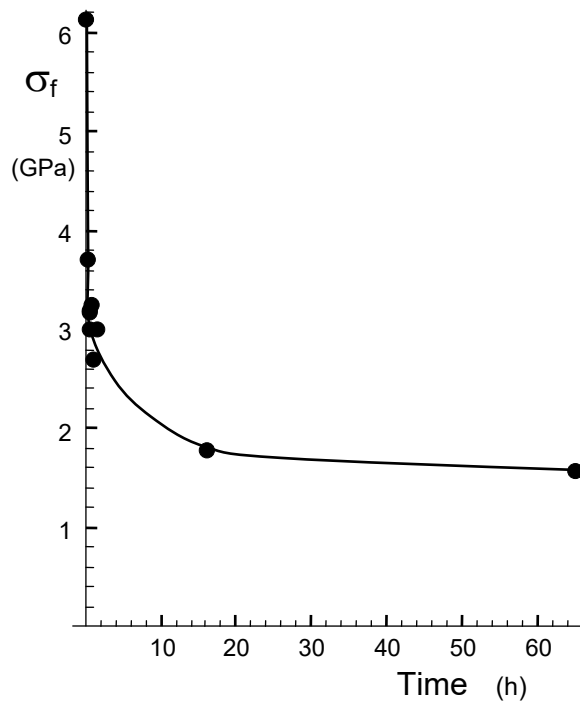## 2. Inert strength

In the case of high-strength silica fibers the inert tensile strengths measured in liquid nitrogen is in the order of about $\sigma_c \cong 12$ GPa. Figure 4 shows results by Inniss et al. [3] (right red straight line). Tests in lab air show clearly lower strengths σ_f which are about 50% of the inert strength, slightly depending on the loading rate. Results by Inniss et al. [3] and Lezzi et al. [2] are represented by the two coinceding left straight lines. The inert strengths for the measurements by Proctor et al. [1] and Lezzi et al. [2] can be computed from the strengths in humid air by well-known relations.

For use of simple equations, we describe the subcritical crack growth rates $v(K)$-behaviour by the power-law relation

$$v = A\,K_I^n = A*\left(\frac{K_I}{K_{Ic}}\right)^n \tag{1}$$

with the parameters A, $A*$ and n depending on the material, the temperature and the environment.
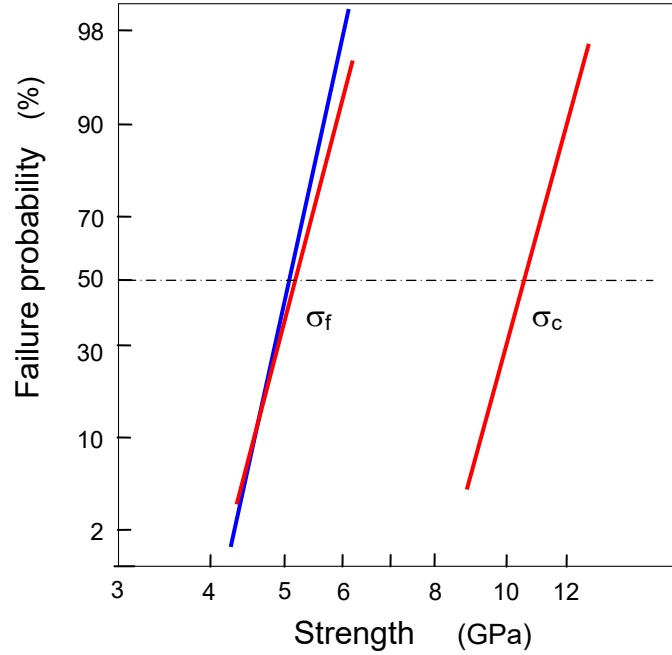
Fig. 4 Strength on silica fibers; σ_f=strength in lab air at 20°C, σ_c=inert strength in liquid N_2 (red: Inniss et al. [3], blue: Lezzi et al. [2]).

Using the power-law approximation of subcritical crack growth. eq.(1), the relation between humidity-affected strength σ_f and inert strength σ_c is given by

$$\sigma_f^{n+1} = B\sigma_c^{n-2}\dot{\sigma}(n+1) \tag{2}$$

In eq.(2) the stress rate is $\dot{\sigma}=d\sigma/dt$ and the material parameter B is defined by

$$ B = \frac{2}{AY^2(n-2)} K_{\mathrm{Ic}}^{2-n} = \frac{2K_{\mathrm{Ic}}^2}{A^*Y^2(n-2)} \; . \tag{3}$$

where $K_{\mathrm{Ic}} \cong 0.75$ MPa$\sqrt{\text{m}}$ is fracture toughness and Y is the geometric function of $Y \approx 1.3$. From results by Wiederhorn and Bolz [4], we determined for $\approx$5-10 Torr water vapour pressure:

$$ n = 41 \, , \; A^* \approx 13.2 \text{ m/s} \Rightarrow B = 0.0013 \text{ MPa}^2 \text{ s} \, . \tag{4}$$

By using eq.(2), the inert strength σ_c can now be computed from the measured σ_f. This was done for the experimental data in Fig. 1 with the results shown in Fig. 5a. The solid symbols represent the measured data and the open symbols the inert strengths. In addition, the experimental results for the two types of strength by Inniss et al. [3] are introduced by the blue triangles. The agreement of measured and computed inert strength with the predicted ones is obvious.

We did the same for the data in Fig. 3 with the result plotted in Fig. 5b. The unknown loading rate for the experimental strength measurements was varied in Fig. 5c assuming that a few seconds were necessary to reach failure. The predictions are hardly affected.
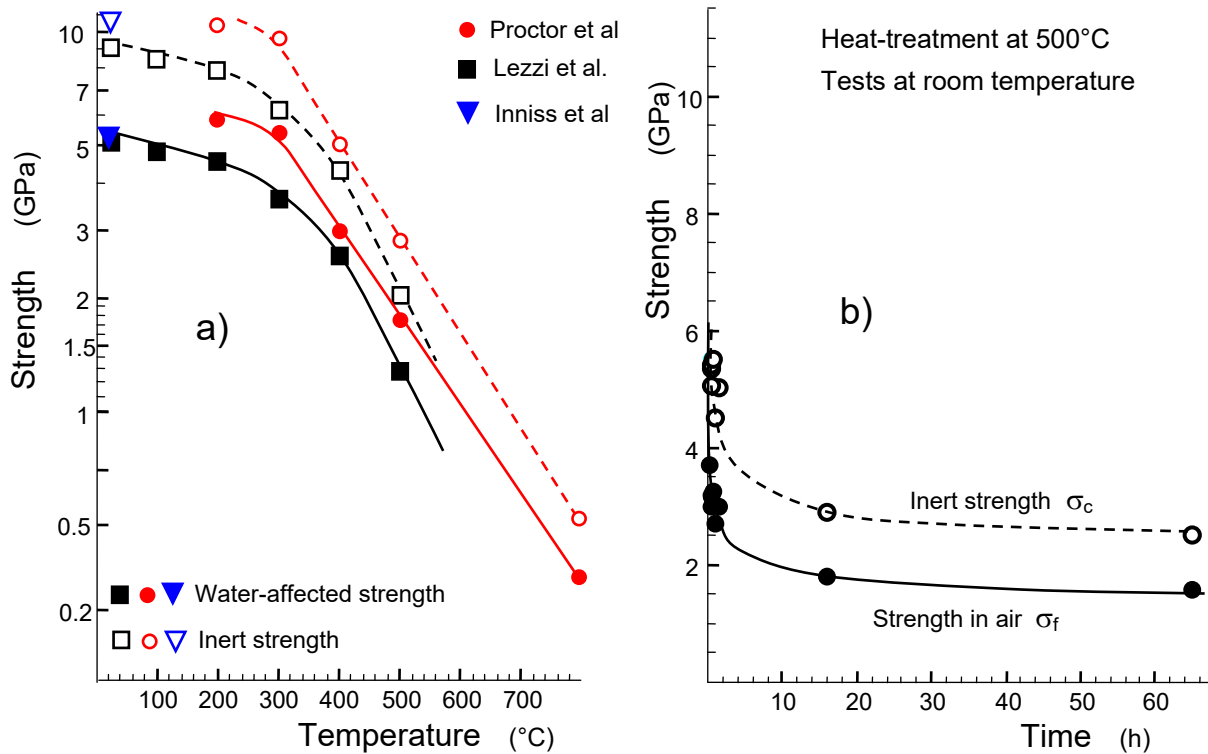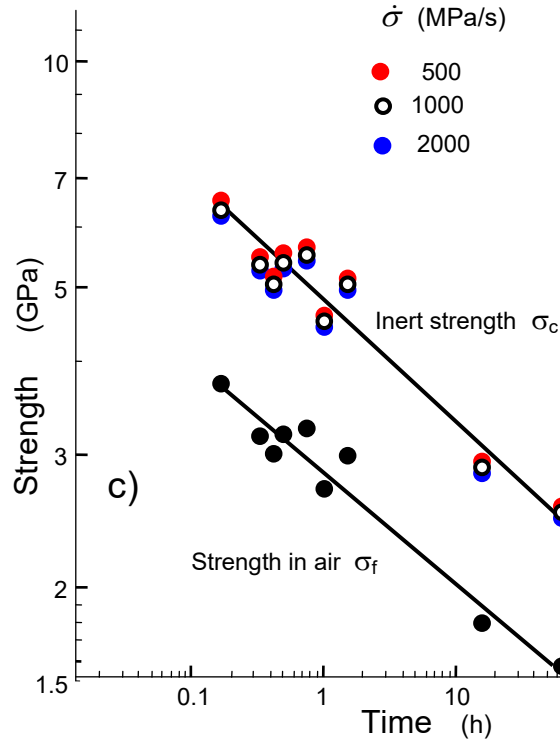
Fig. 5 a) Inert strengths of silica fibres computed from data by Proctor et al. [1] and Lezzi et al. [2] vs. temperature. Triangles represent strength measurements by Inniss et al. [3] in humid air and liquid nitrogen; b) strengths in humid air by Proctor et al. [1] (solid circles) and inert strengths (open circles) as a function of heat-treatment time at 500°C, c) strength data in logarithmic representation, effect of the loading rate.

3 Consequences from results by Proctor et al.

3.1 Strength and pore size

From the inert strengths of Fig. 5a, we interpolated the data for the additional temperature of 600°C as compiled in the column 3 of Table 1. The related sphere radii are introduced in the 4th column of Table 1. Column 5 shows the products of inert strength σ_c and damage radius R.

Temperature	σ_f (GPa)	σ_c (GPa)	R (μm)	$\sigma_c \times R$ (MPa mm)	a_f (μm)	a_c (μm)
600°C	1.05	1.62	7.6	12.31	0.031	0.013
800°C	0.37	0.53	22.4	11.87	0.265	0.125

Table 1 Strengths from Fig. 5a and radii for semi-spherical pores [1] at 600 and 800°C.

The products in column 5 of Table 1 are sufficiently constant, $\sigma_c \times R \approx 12$ MPa mm. Consequently, it can be roughly approximated

$$R \approx \frac{12\,\text{MPa mm}}{\sigma_c} \tag{5}$$

5

The result of the dependence $\sigma_c = f(R)$, namely $\sigma_c \propto 1/R$, is not trivial as will be shown below.

Figure 6 shows the inert strength σ_c at 500°C as the black curve. The red curve and red symbols represent the radius of the damaged zone under the assumption that eq.(5) is fulfilled even for 500°C.
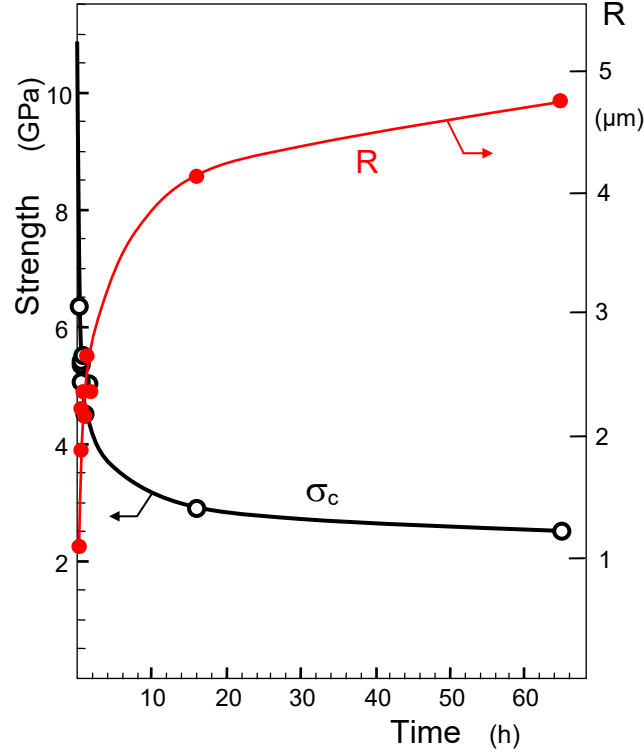

Fig. 6 Inert strength and damage radius for 500°C heat-treated fibers assuming eq.(5) also at this lower temperature.

3.2 Pore model

The damaged zone in Fig. 2 is strongly cracked by irregularly oriented cracks. This region cannot carry external load. It may be modelled as a hemisphere with disappearing Young's modulus, $E \cong 0$, located in an intact material with normal modulus, i.e. $E = 72$ GPa.

Figure 7a shows a symmetry element of a two-dimensional array of semi-spherical pores at a flat surface. The radius of the half-sphere is R and the distance to the next one $2H$. The applied stress is denoted as σ_∞. The stresses σ_y along the equator between points (A) and (B) are represented in Fig. 7b for several values of H/R. It has to be noted that the stress concentration k depends on the relative size of the symmetry elements R/H, but not on the absolute value of R.

From the pore model we have to expect failure when the maximum tangential stress at the pore, σ_{max}, equals a critical value σ^{cr}. When k denotes the stress concentration

factor at the deepest point of the half-sphere and again σ_c is the inert strength, it must hold at failure

$$\sigma_c = \frac{\sigma^{cr}}{k} \qquad (6)$$

The maximum concentration factor is $k \cong 2$. From this point of view, not any influence of pore size on strength should exist, in contrast to the experiment.

The maximum possible stress at the circumference of a pore is reached, when the critical stress σ^{cr} equals the theoretical strength σ_0 that is for silica $\sigma_0 = 23$ GPa [5]. Consequently, it results for the maximum possible strength according to eq.(6)

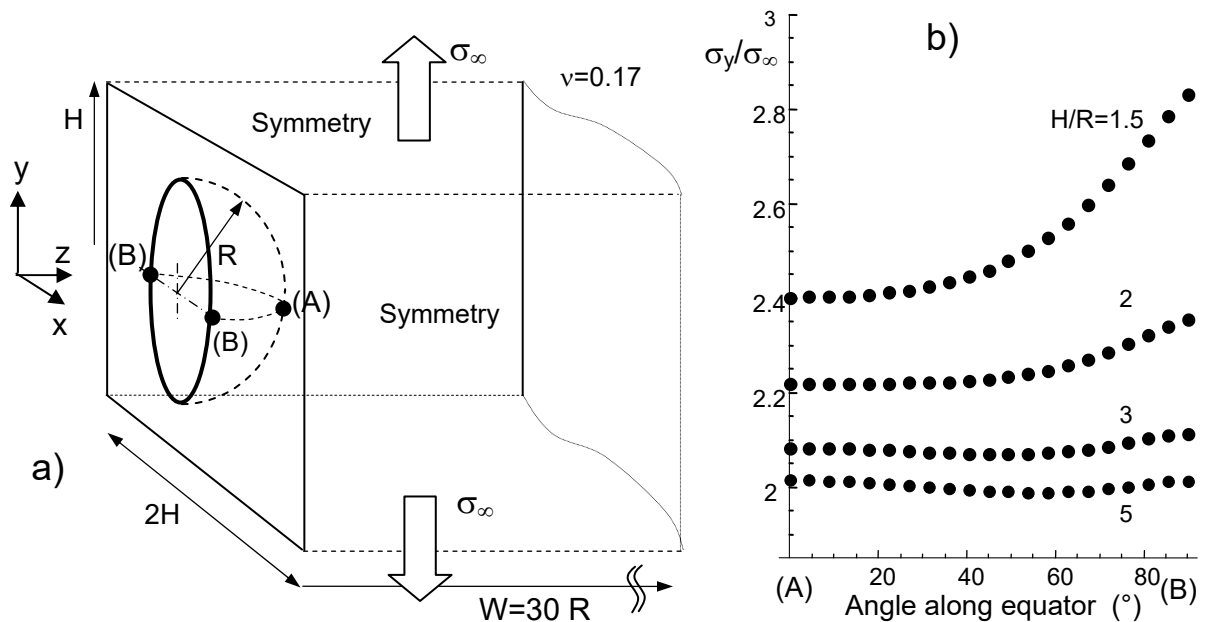$$\sigma_{c,max} = \frac{\sigma_0}{k} = \frac{23\,\text{GPa}}{2} = 11.5\,\text{GPa} \qquad (7)$$

Fig. 7 a) Semi-spherical surface pore under uniaxial loading, b) stress distribution σ_y along the equator, surface: (B), deepest point: (A).

3.3 Pore/crack model

Strength behaviour of pore-like defects is in fracture mechanics described by an open pore of radius R with a fictive annular crack of depth a normal to the applied stress as was suggested by Baratta [6,7], Fig. 8. The size of the fictive crack can experimentally estimated from the pore-radius, the fracture toughness of the undamaged material and the measured strength.

In a fracture mechanics description of the dependency strength vs. crack size,

$$\sigma_c = \frac{K_{Ic}}{F\sqrt{\pi a}} \tag{8}$$

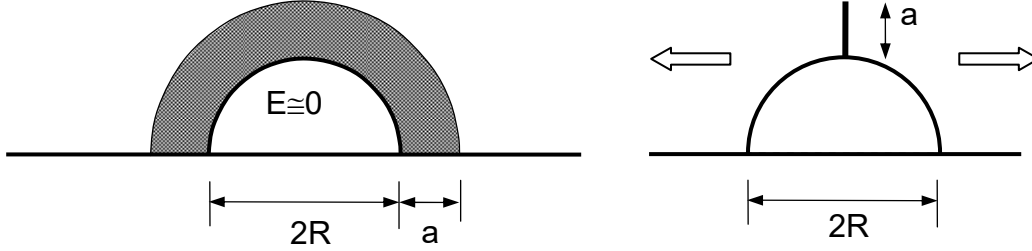the strength would become infinite for disappearing crack depth, $a\to 0$.

Fig. 8 Semi-spherical void with a fictive circumferential crack normal to the applied stress in a tensile strength test.

The fact of a limited strength can simply be incorporated by an intrinsic crack size a_0 leading to $\sigma_c = \sigma_{c,max}$ as is fulfilled by

$$\sigma_{c,max} = \frac{K_{Ic}}{F\sqrt{\pi a_0}} \tag{9}$$

yielding the intrinsic crack depth as

$$a_0 = \frac{1}{\pi}\left(\frac{K_{Ic}}{F\sigma_{c,max}}\right)^2 \tag{9a}$$

For a very small crack depth, $a_0 \ll R$, we obtain with $F=2.25$, $K_{Ic}=0.8$ MPa$\sqrt{m}$, and $\sigma_{c,max}=11500$ MPa a very small pre-existent crack depths of $a_0=0.3$ **nm**. This depth agrees well with the size of the silica rings, below which the application of continuum mechanics doesn't make any sense.

The strength in presence of a circumferential crack, $\sigma_c < \sigma_{c,max}$, then holds

$$\sigma_c = \frac{K_{Ic}}{F\sqrt{\pi(a+a_0)}} \tag{10}$$

The stress intensity factor for the circumferentially cracked semi-spherical surface void under equi-biaxial stresses was studied by Baratta [6] and Zhu et al. [8]. In [8] an equation is given for the Poisson's ratio of $\nu=0.25$ that reads for the stress intensity factor at the circumference of the hemisphere:

$$K = F\sigma\sqrt{\pi a} \tag{11}$$

For uniaxial stresses we found by a Finite Element analysis with $\nu=0.17$: $k\approx 2.0$ [9]. The geometric function can be fitted as

$$F = (1.12 - 0.22\arctan[a/R])(1 + 1.02\exp[-5.14\,a/R])\,. \tag{12}$$

Since the ratio a/R is for the data in Table 1 $a/R < 0.012$, the geometric function F simplifies to

$$F \approx k \times 1.12 \approx 2.24 \tag{13}$$

i.e. twice the geometric function of the edge-cracked half-infinite body. This implies that the strength of the pore-like damaged silica surface is about half of the strength of a smooth silica fiber surface containing the same defect population. The 6th and 7th columns of Table 1 contain the crack sizes at failure.

In order to demonstrate the relationship between crack length, geometry function and strength, we want to arbitrarily calculate the (theoretical) inert strength and the course of the fracture mechanical geometry function for a pore with the radius $R = 20$ µm. Figure 9 shows the results. From Fig. 9a it can be concluded, that up to $a \approx 10^{-7}$m an influence of the crack size on the geometric function can be ignored. Figure 9b shows the inert strengths as the continuous curve in comparison with the two limit-case solutions for the geometric function in Fig. 9a, introduced by the dash-dotted straight lines.
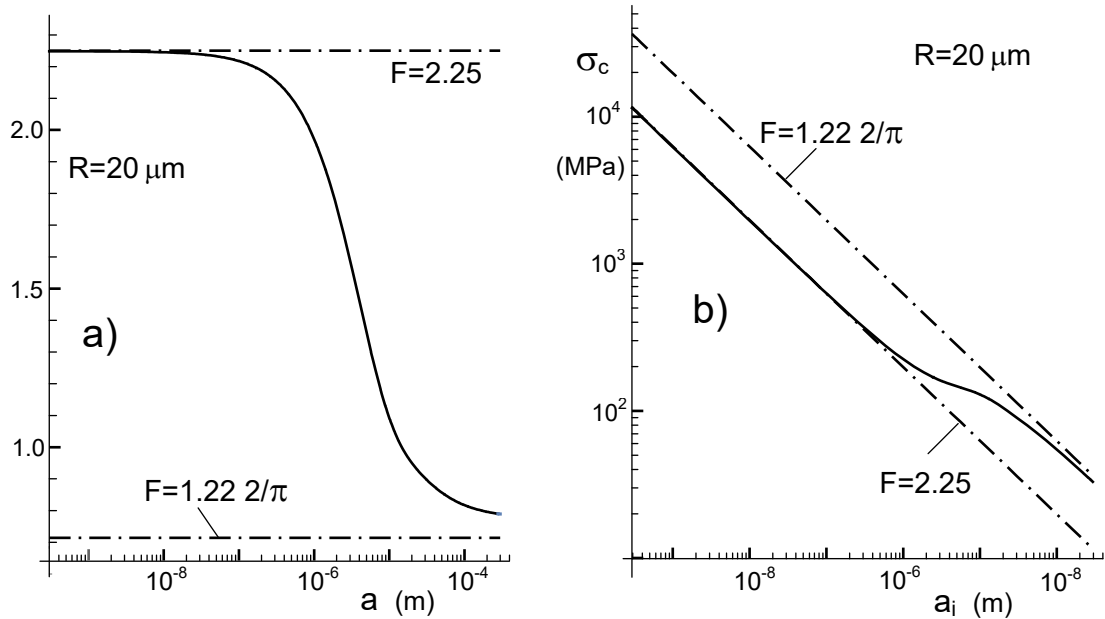

Fig. 9 a) Geometric function F vs. crack length a, b) inert strength versus initial crack length a_i. Straight lines: limit cases with constant F, from Fig. 9a.

3.4 Computation of strength

For the computation of strength, we need the value of fracture toughness. This property is in the surface damaged state of course not a constant value. In the pore it

trivially disappears. Outside the pore it doesn't rise abruptly to the value of silica. Via diffusion, the reaction products are present even under the pore surface, resulting in a toughness distribution as is illustrated schematically in Fig. 10. This figure shows a surface "pore" generated due to the reaction between dust particles on the surface and the silica. Consequently, local toughness K'_{Ic} increases from $K'_{Ic}=0$ at the pore surface to the value $K'_{Ic}=K_{Ic}$ in the bulk material. Fracture of this region by an increasing uniaxial stress causes a ring-shaped crack with the depth continuously increasing until the failure condition for the bulk material $K_{appl}=K_{Ic}$ is reached. Diffusion depth d of the reaction products into the surrounding material depends on time t

$$b = \sqrt{Dt} \qquad (14)$$

where D denotes the diffusivity of reaction product in silica. The crack length at fracture should correspond at least approximately to the diffusion length b. Therefore, we set $a=b$.
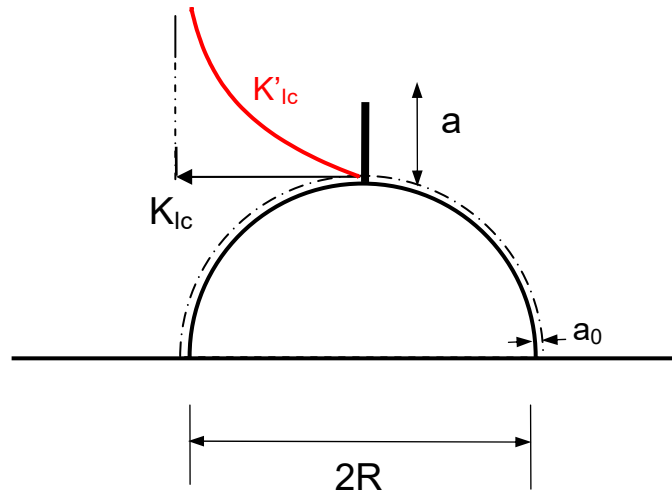

Fig. 10 Surface "pore" due to reaction between dust particles and silica. Toughness K'_{Ic} increase from $K'_{Ic}=0$ at the pore surface to the value $K'_{Ic}=K_{Ic}$ in the bulk material.

Next we fitted the dependency of inert strength vs. heat-treating time t. Use of Least-squares fitting procedure by Mathematica [10] yields the parameters a_0 and D

    Intrinsic crack depth a_0=**6.09 10^{-10} m** [3.9 10^{-10}, 8.3 10^{-10}]

    equivalent to a maximum strength of $\sigma_{c,max}$=**7135 MPa** [6145, 8960]

    and the diffusivity $\mathbf{log_{10}}$ $\boldsymbol{D}$**=-21.9** [-22.6, -21.6] (for D in m^2/s**)**

with the 90% Confidence Intervals in brackets. The related fitting curve is given in Fig. 11 together with the data points.

σc

8000

6000

(MPa)
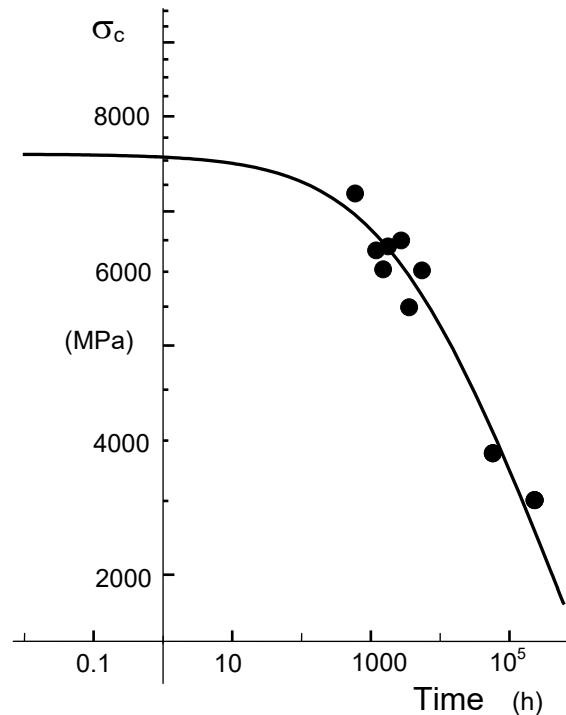
4000

2000

0.1   10   1000 10^5

Time (h)

Fig. 11 Data fit, curve: computed with best fitting parameter set.

References

1 A. Proctor, I. Whitney, J.W. Johnson, The strength of fused silica, Proceedings of the Royal Society of London. Series A. Mathematical and Physical Sciences, Vol. 297, No. 1451 (1967), 534-557.

2 P.J. Lezzi, Q.R. Xiao, M. Tomozawa, T.A. Blanchet, C.R. Kurkjian, Strength increase of silica glass fibers by surface stress relaxation: A new mechanical strengthening method, J. of Non-Crystalline Solids **379** (2013) 95–106.

3 D. Inniss, Q. Zhong, C.R. Kurkjian, Chemically corroded pristine silica fibers: Blunt or sharp flaws?, J. Am. Ceram. Soc. **76**(1993), 3173-77.

4 Wiederhorn, S.M. and Bolz, L.H., Stress Corrosion and Static Fatigue of Glass, J. Am. Ceram. Soc. **53**[10] (1970), 543-548.

5 Silva, E. C. C. M.; Tong, L.; Yip, S.; Van Vliet, K. J. *Small* **2006**, *2*, 239–243.

6 Baratta, F.I., Stress intensity factor estimates for a peripherally cracked spherical void and a hemispherical surface pit, J. Am. Ceram. Soc. **61**(1978), 490-493.

7 Baratta, F.I., Mode-I stress intensity factor estimates for various configurations involving single and multiple cracked spherical voids, Fracture Mechanics of Ceramics, Vol. 5, Plenum Press, 1983, 543-567.

8 Zhu, G.Q., Ritter, J.E., Jakus, K., Bhattacharya, S., Stress intensity factor for a peripherally cracked spherical cap, J. Am. Ceram. Soc. **80**(1997), 2445-48.

9 G. Rizzi, T. Fett, Defects at silica surfaces and crack-tip shielding- A Finite Element Study, **33**, 2015, ISSN: 2194-1629, Karlsruhe, KIT.

10 *Mathematica*, Wolfram Research, Champaign, USA.